


## Research Article

# Evaluation of Gamma-Ray Dose Distribution in the Toroidal Direction of LHD Vacuum Vessel from Radionuclides Generated in Deuterium Plasma Experiments

Yasuyuki Ogino <sup>1,2</sup>, Makoto I. Kobayashi,<sup>3,4</sup> Keisuke Mukai,<sup>2</sup> Juro Yagi,<sup>2</sup> Satoshi Konishi,<sup>2</sup> Kunihiro Ogawa,<sup>3,4</sup> and Mitsutaka Isobe<sup>3,4</sup>

<sup>1</sup>Institute for Materials Research, Tohoku University, Sendai, Miyagi 980-8577, Japan

<sup>2</sup>Institute of Advanced Energy, Kyoto University, Uji, 611-0011 Kyoto, Japan

<sup>3</sup>National Institute of Fusion Science, National Institutes of Natural Sciences, Toki, 509-5292 Gifu, Japan

<sup>4</sup>The Graduate University for Advanced Studies, SOKENDAI, Toki, 509-5292 Gifu, Japan

Correspondence should be addressed to Yasuyuki Ogino; [yasuyuki.ogino.b2@tohoku.ac.jp](mailto:yasuyuki.ogino.b2@tohoku.ac.jp)

Received 26 June 2023; Revised 29 August 2023; Accepted 18 December 2023; Published 17 January 2024

Academic Editor: Adrian Loy Chun Minh

Copyright © 2024 Yasuyuki Ogino et al. This is an open access article distributed under the Creative Commons Attribution License, which permits unrestricted use, distribution, and reproduction in any medium, provided the original work is properly cited.

The evaluation of activities from radionuclides inside a vacuum vessel is required for the safe maintenance and estimation of the activation level of fusion devices. The Large Helical Device (LHD), Toki, Japan, has been performing deuterium plasma experiments since 2017, and radionuclides have accumulated in components such as vacuum vessels. In this work, the gamma-ray spectrum and activity of each detected radionuclide in an LHD vacuum vessel were evaluated using portable high-purity germanium (P-HPGe) and numerical calculations of photon transport for comparison with the removed armor tiles to evaluate the occupational exposure in the maintenance of LHD experiments. Measurements using the P-HPGe detector were performed at 20 positions along the toroidal direction of the LHD, at each O port, and between each pair of adjacent O ports. Using the estimated efficiency of the photoelectronic effects inside the P-HPGe detector calculated by Monte Carlo N-particle code version 6.1, the activities of the radionuclides in the armor tiles attached to the vacuum vessel were evaluated. The estimated activity concentrations were compared with the measured activities of the armor tiles removed from the vacuum vessel. Gamma rays from  $^{58}\text{Co}$ ,  $^{54}\text{Mn}$ , and  $^{60}\text{Co}$  were detected, and the measured activities of  $^{58}\text{Co}$  and  $^{54}\text{Mn}$  generated by fast neutrons in the armor tile were almost consistent with those obtained from the removed armor tiles. The radioactivity of  $^{60}\text{Co}$  in the armor tile was underestimated compared with the activity obtained from the removed armor tiles. The measurement of activation by fast neutrons is feasible, whereas activation by thermal neutrons requires more accurate calculations and surveys to be measured using this method.

## 1. Introduction

Radiation analysis is required for the safe operation of plasma devices and fusion reactors in which deuterium and tritium plasma operations are performed. The vacuum vessels, plasma-facing walls, and components of such systems are activated, and specific radionuclides accumulate inside them. The accumulation of radionuclides is a problem related to the maintenance, replacement cycle, performance degradation of components, and decommissioning of

devices. Simulations and analyses of activation by fusion neutrons have been reported, which have focused on the prediction of radioactive waste and its regulation [1, 2]; estimation and experiments of hydrogen isotopes inside the whole system of fusion devices or their plasma-facing walls, divertors, and components [3, 4]; and comparison between fission and fusion power plants [5]. In particular, predictions at the decommissioning step are essential because specific radionuclides with long half-lives (several years) accumulate inside the components. However, the geometry of the

components in simulations is usually simplified and has uncertainties, which may result in discrepancies between the simulation results and the actual accumulation. Therefore, the radioactivity obtained from simulations and actual environments should be compared as a benchmark test to improve the accuracy and reliability of the simulation results.

The Large Helical Device (LHD), an experimental fusion plasma device located in Toki, Japan, started deuterium–deuterium (DD) plasma experiments in 2017. The LHD is a helical-type plasma device and is equipped with a negative-ion-based neutral beam injector (N-NBI) to sufficiently increase the ion and electron temperatures for DD fusion reactions. The DD plasma experiments contribute to analyzing the hydrogen isotope effect in plasma confinement and the upgraded heating device of NBIs, investigating the confinement property of energetic particles in helical plasmas, and extending the plasma-material interaction using the steady-state operability of the LHD [6]. Each DD plasma experiment generated neutrons at a rate of  $10^8$ – $10^{18}$  neutrons/s, which were monitored by fission chambers with  $U_2O_3$ . To ensure safety, such as the replacement of components and maintenance of devices, the accumulation of radionuclides must be predicted. For safe maintenance, occupational radiation exposure inside a vacuum vessel was monitored in a previous study [7]. To evaluate the neutron flux distribution of the fusion devices, neutron activation analysis was conducted using material foils and a two-dimensional radiation dosimeter in the torus hall in which the LHD was installed [8]. According to this report, fusion neutrons spread around the LHD; neutrons were detected using material foils inside the torus hall during deuterium operations in 2017, and the successful measurement of the distribution of thermal and epithermal neutrons was reported. Differences existed in the thermal neutron fluxes with the component layout in the torus hall, and a uniform distribution of fast neutrons was observed near the LHD. In contrast, the distribution of thermal neutrons was nonuniform because of the thermal neutron absorber underneath the specific port of the vacuum vessel. Based on this result, the difference in the neutron flux distribution may make the activation of a fusion device disproportionate, which is an important issue for maintenance.

For safety management, gamma-ray spectrometric measurements and dose rate evaluations were conducted using an NaI(Tl) survey meter aimed at the activated armor tiles removed from the LHD vacuum vessel [9]. This method is highly effective for low-level activation components. However, highly activated and dust-polluted components are difficult to measure by extraction and require estimation prior to extraction. Hence, a technique to measure the radiation of the device remotely needs to be developed for a fusion reactor in such an inaccessible environment, and it must be applicable to inspection robotics inside a vacuum vessel.

Based on previous research, the gamma rays emitted from the radionuclides generated by neutrons in an LHD vacuum vessel were measured in this study and compared with the measured activity of the removed armor tiles. To calculate the activities from the in situ measurements, a photon transport simulation was conducted to obtain the efficiency of the photoelectric effect.

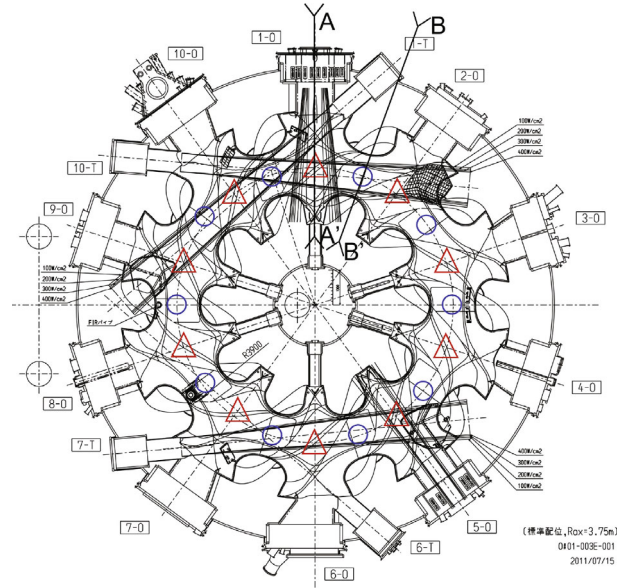


FIGURE 1: Toroidal configuration of LHD and measurement positions. Blue circles indicate U/L ports, and red triangles indicate O ports.

TABLE 1: Detected radionuclides, gamma-ray energies, emission possibilities, and activities  $A_2$  of removed armor tiles [9].

Nuclide	Energy (keV)	$r_\gamma$	$A_2$ (at U/L port) (Bq/g)
$^{58}\text{Co}$	811	0.995	$2.13 \pm 0.06$
$^{54}\text{Mn}$	835	1	$1.56 \pm 0.06$
$^{60}\text{Co}$	1173	0.999	$1.06 \pm 0.06$
	1332	1	$1.12 \pm 0.06$

## 2. Methods

A portable high-purity germanium (P-HPGe)-based radionuclide identifier (Falcon 5000, Mirion Technologies, Canberra) was employed to measure the gamma rays inside the vacuum vessel of the LHD. The P-HPGe detector was composed of single-crystal germanium (60.8 mm in diameter and 31 mm in thickness) covered with an aluminum holder and equipped with an electromechanical cooling system.

The in situ measurements using the P-HPGe detector were performed at 20 positions along the toroidal direction of the LHD for every O port and between each pair of adjacent O ports, called the upper/lower (U/L) ports, as shown in Figure 1. There are horizontal spaces for O ports and vertical spaces for U/L ports for diagnostics, heating devices, maintenance, or vacuum systems. The P-HPGe detector was mounted on the equatorial plane of the maintenance rail, which was 5.5 m above the ground level of the torus hall, and the P-HPGe detection port was directed toward the toroidal direction at every position. The measurement duration at each position was set to 240 s as the live time at port 1 and 180 s at the other positions. The measurements were performed on June 17, 2020, 132 days after the last plasma experiment in the 21st cycle.

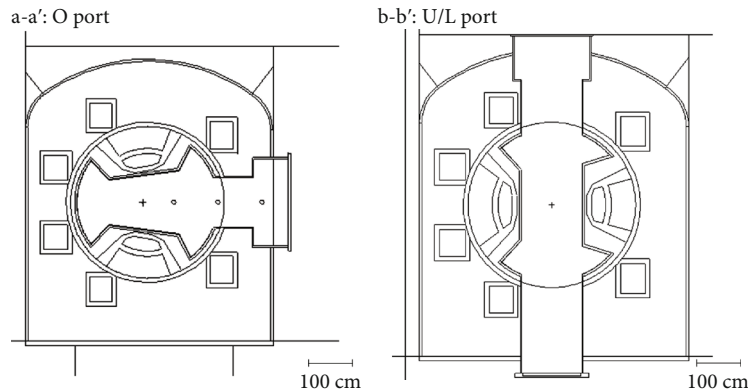


FIGURE 2: Sectional views in a-a' and b-b' from Figure 1 drawn by Visual Editor based on the LHD geometry for MCNP calculation.

The activity concentration of radionuclide  $A_1$  (Bq/g), measured using the P-HPGe detector inside the vacuum vessel, was calculated using the following equation:

$$A_1 = \frac{c}{r_\gamma M p}, \quad (1)$$

where  $c$  (/s) is the count rate of each photoelectric peak by the specific gamma rays from the radionuclide measured by the P-HPGe detector,  $r_\gamma$  is the radionuclide emission probability of each gamma-ray,  $M$  (g) is the mass of armor tiles inside the vacuum vessel, and  $p$  is the photopeak efficiency obtained by photon transport calculation. The typical weight of each armor tile was 1500–1600 g, and 7200 armor tiles were attached to the inner surface of the vacuum vessel. The thickness of the armor tiles was 0.5 cm. In this study, the weight of each armor tile was set to 1600 g. The coincidence summing effect should be considered for specific radionuclides, particularly  $^{60}\text{Co}$ . Because the distance between the detector and the inner surface of the vacuum vessel was approximately 1 m, such effects were negligible in this study.

The radioactivity obtained by an armor tile removed from the vacuum vessel at the 1–2 U/L port was also evaluated using the same P-HPGe detector [9]. One armor tile leaned on the wall of the torus hall, approximately 30 m away from the LHD cryostat, and the P-HPGe detection port was attached to one side of the tile. At this time, the collimator (8 mm-thick tungsten polymer) was used to reduce the environmental gamma rays. Table 1 shows the measured gamma-ray energy, emission probabilities  $r_\gamma$ , and activity concentrations of  $A_2$  for each radioactive nuclide whose values were already reported by Kobayashi et al. [9].

To evaluate the photoelectric effect, photon transport calculations were performed using Monte Carlo N-particle (MCNP) code version 6.1 [10]. The simulated geometry was based on the model of Nishitani et al. [11], and the cells for the armor tiles were attached to the inner surface of each segment of the vacuum vessel. The LHD geometry was composed of two types of repeating units corresponding to the O port and U/L port by  $18^\circ$ . As shown in Figure 2, for each sectional view in a-a' and b-b' drawn using Visual Editor, the cell of the germanium detection port was located at the cen-

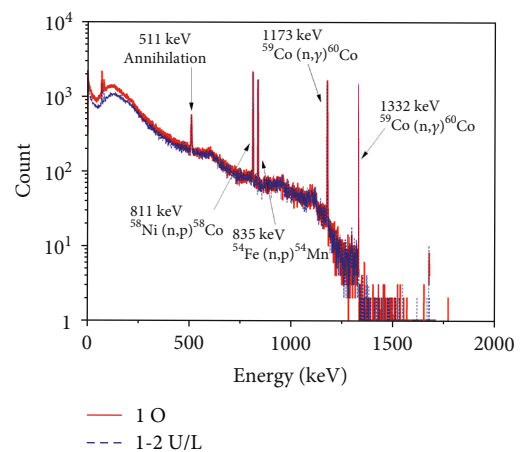


FIGURE 3: Gamma-ray energy spectrum counted by P-HPGe. The red line indicates the measured data at the 1 O port, and the blue dotted line indicates the measured data at the 1–2 U/L port.

ter of each port. In the vacuum vessel of the calculation geometry, the maintenance rail was not defined, and the P-HPGe detector was defined only as a germanium crystal, excluding the device housing. The source was defined as an isotropic and monochromatic photon in the cells of the armor tiles. The MCPLIB04 library was used for the photoatomic reaction calculations [12]. The photopeak efficiency inside the germanium crystal was calculated using the F8 pulse height tally option, which is an estimator used to score the particles entering the cell with the source weight of its energy. The number of simulation histories was set to  $5 \times 10^7$  to avoid exceeding a relative error of 0.20. The material of the cells for the armor tiles was set as SUS316L in the simulation, although some of the actual armor tiles were replaced with graphite, molybdenum, and tungsten near the neutral beam injection ports or divertor [13, 14].

### 3. Results

Figure 3 shows the gamma-ray energy spectra measured at the 1 O and 1–2 U/L ports inside the vacuum vessel. Peaks at 811, 835, 1173, and 1332 keV are evident, corresponding to the radionuclides  $^{58}\text{Co}$ ,  $^{54}\text{Mn}$ , and  $^{60}\text{Co}$ , respectively.

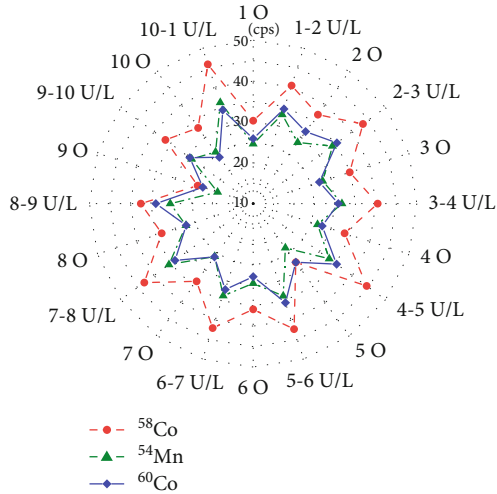


FIGURE 4: Toroidal distribution of gamma-ray count rates measured by the P-HPGe detector.

The peak at 511 keV was generated by pair annihilation inside or outside the Ge crystal. These radionuclides were mainly generated by transmutations of  $^{58}\text{Ni}(n,p)^{58}\text{Co}$ ,  $^{54}\text{Fe}(n,p)^{54}\text{Mn}$ , and  $^{59}\text{Co}(n,\gamma)^{60}\text{Co}$ . The detected radionuclides shown in Figure 3 are the same as those listed in Table 1, and these transmutations are predominantly from the materials of the armor tiles, vacuum vessels, and components. Armor tiles and vacuum vessels are composed of SUS316L, which mainly contains 16–18 wt.% of Cr, 12–15 wt.% of Ni, 2–3 wt.% of Mo, and 2 wt.% of Mn, which was activated by neutrons during deuterium operation. A weak peak was detected between 73 and 75 keV. However, radionuclides were not identified in this peak because many candidates corresponded to this energy region in the database.

Figure 4 shows the toroidal distribution of the count rates of each radionuclide,  $^{58}\text{Co}$ ,  $^{54}\text{Mn}$ , and  $^{60}\text{Co}$ , measured using the P-HPGe detector. The count rate tends to increase at each U/L port, in contrast to each O port. The count rate of  $^{58}\text{Co}$  is the highest among the radionuclides at every position, whereas the count rates of  $^{54}\text{Mn}$  and  $^{60}\text{Co}$  are similar. The count rates of  $^{58}\text{Co}$  at the 4–5 and 10–1 U/L ports are slightly higher than those at the other positions. The count rates of all radionuclides, particularly  $^{54}\text{Mn}$ , at ports 5 and 9 are slightly lower than those at the other positions. Figure 5 shows the activity of each detected nuclide, whose values were calculated using Eq. (1), and Table 2 lists the activation reactions, energy of each gamma-ray, count rate measured inside the vacuum vessel, activities  $A_1$ , and ratio of  $A_1$  and  $A_2$  with the respective errors. The measured results for the count rate are only shown for the 1 O and 1–2 U/L ports because of the symmetry of the calculation geometry. The activities were calculated by applying Eq. (1) with the count rate, gamma-ray emission possibility, and photopeak efficiency calculated by using the MCNP code. The obtained values of  $A_1$  at 811 and 835 keV are approximately equivalent to the values of  $A_2$ , and the values of  $A_1$  at 1173 and 1332 keV are 1.78–3.36 times higher than those of  $A_2$ .

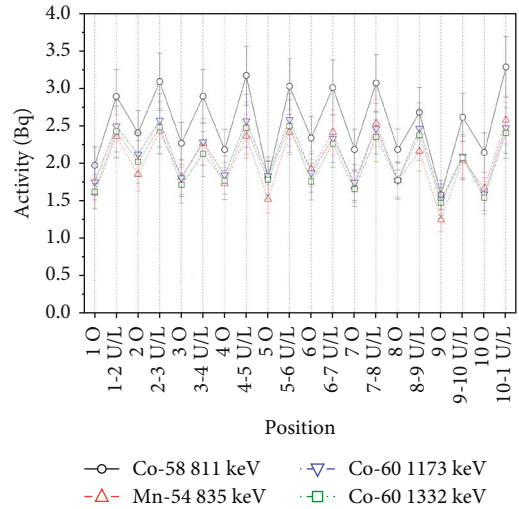


FIGURE 5: Measured activity of detected radionuclides calculated by Eq. (1) at every port position.

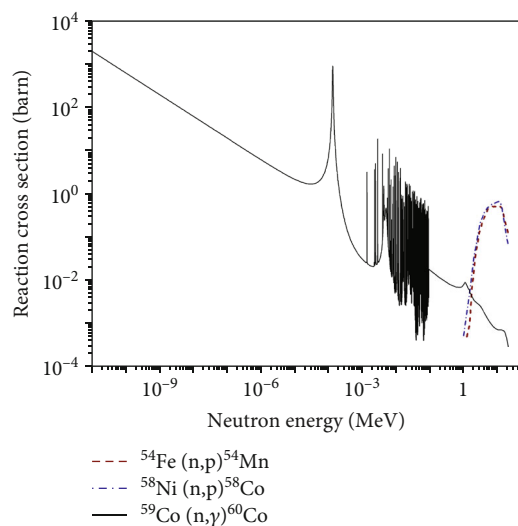
#### 4. Discussion

As shown in Figure 4, the radionuclides  $^{58}\text{Co}$ ,  $^{54}\text{Mn}$ , and  $^{60}\text{Co}$  were detected. Both the  $^{58}\text{Ni}(n,p)^{58}\text{Co}$  and  $^{54}\text{Fe}(n,p)^{54}\text{Mn}$  transmutations are threshold reactions from the neutrons of approximately 1 and 1.25 MeV shown in Figure 6 [15]. Based on these reaction cross-sections, the (n,p) reactions mainly occurred with fast neutrons originating from the deuterium–deuterium fusion reaction of 2.45 MeV. The  $^{59}\text{Co}(n,\gamma)^{60}\text{Co}$  reaction mainly occurs with thermal neutrons through multiple scattering and attenuation both inside and outside the LHD. In our cases, the detected radionuclides  $^{58}\text{Co}$  and  $^{54}\text{Mn}$  were distributed around the LHD vacuum vessel, and  $^{60}\text{Co}$  was distributed not only around the vacuum vessel but also around the components of the divertors, maintenance ports, coils, diagnostics, and supports.

The peak at approximately 122 keV reported in two previous papers [9, 16] is not evident in Figure 3. This peak originated from the  $^{58}\text{Ni}(n,d)^{57}\text{Co}$  and  $^{58}\text{Ni}(n,np)^{57}\text{Co}$  transmutations, which emitted gamma rays of 122 keV with a half-life of 271 d. The  $^{58}\text{Ni}(n,d)^{57}\text{Co}$  and  $^{58}\text{Ni}(n,np)^{57}\text{Co}$  reactions are threshold reactions that occur with neutrons above 8 and 9.5 MeV, respectively. A small number of deuterium–tritium (DT) fusion reactions has been reported to occur during the DD operation in LHD [17], which results in the activation of fast neutrons. This peak was clearly detected in the DT fusion reactor, which is an important criterion for evaluating activation by fast neutrons [18]. Another possible cause of this peak is the decayed gamma ray of 122 keV from  $^{152}\text{Eu}$ , which contains impurities in concrete [19, 20]. In these measurements, the measured positions were distant from the concrete wall of the torus hall, and the high radiation dose rate resulted in Compton scattering, making it difficult to find a peak in the low-energy region. The measured positions inside the LHD vacuum vessel were far from the concrete, and the DT fusion reaction neutrons were so small that the transmutation of

TABLE 2: Activities of radionuclides measured by the P-HPGe detector and ratio of  $A_1$  and  $A_2$ .

Port	Primary reaction	Energy (keV)	$c$ (/s)	$p$ (10-6)	$A_1$ (Bq/g)	Ratio ( $A_1/A_2$ )
1 O	$^{58}\text{Ni}(n,p)^{58}\text{Co}$	811	$30.3 \pm 0.6$	$1.34 \pm 0.16$	$1.97 \pm 0.25$	$0.92 \pm 0.11$
	$^{54}\text{Fe}(n,p)^{54}\text{Mn}$	835	$24.6 \pm 0.6$	$1.36 \pm 0.16$	$1.57 \pm 0.19$	$1.00 \pm 0.13$
	$^{59}\text{Co}(n,\gamma)^{60}\text{Co}$	1173	$26.9 \pm 0.7$	$1.12 \pm 0.15$	$2.09 \pm 0.29$	$1.96 \pm 0.29$
	$^{59}\text{Co}(n,\gamma)^{60}\text{Co}$	1332	$24.9 \pm 0.7$	$1.08 \pm 0.14$	$2.00 \pm 0.28$	$1.78 \pm 0.26$
1-2 U/L	$^{58}\text{Ni}(n,p)^{58}\text{Co}$	811	$40.3 \pm 0.9$	$1.22 \pm 0.15$	$2.89 \pm 0.38$	$1.35 \pm 0.18$
	$^{54}\text{Fe}(n,p)^{54}\text{Mn}$	835	$32.9 \pm 0.8$	$1.18 \pm 0.15$	$1.42 \pm 0.32$	$1.55 \pm 0.21$
	$^{59}\text{Co}(n,\gamma)^{60}\text{Co}$	1173	$34.8 \pm 1.0$	$0.92 \pm 0.13$	$3.25 \pm 0.49$	$3.10 \pm 0.49$
	$^{59}\text{Co}(n,\gamma)^{60}\text{Co}$	1332	$33.8 \pm 1.0$	$0.78 \pm 0.12$	$3.82 \pm 0.62$	$3.36 \pm 0.57$

FIGURE 6: Reaction cross-sections of  $^{58}\text{Ni}(n,p)^{58}\text{Co}$ ,  $^{54}\text{Fe}(n,p)^{54}\text{Mn}$ , and  $^{59}\text{Co}(n,\gamma)^{60}\text{Co}$  drawn by JENDL-4.0 [15].

$^{58}\text{Ni}(n,np)^{57}\text{Co}$  did not occur. Hence, no peaks were detected in a channel equivalent to 122 keV in this study.

As explained above, in Figure 4, the count rates of  $^{58}\text{Co}$  at the 4-5 and 10-1 U/L ports are slightly higher than those of the others. However, the count rates of  $^{54}\text{Mn}$  are not significantly different between the O and U/L ports. The shielding tiles covering the wall around the NBI ports were composed of graphite, and some SUS316L tiles were replaced during the maintenance periods. Because a precise irradiation history was not considered in this study, we cannot say that there are significant differences in the count rates between the positions around the NBIs.

In Table 2, activities  $A_1$  of 811 and 835 keV are almost in agreement with activities  $A_2$ , whereas the  $A_1$  values of 1173 and 1332 keV are 1.78-3.36 times higher than the  $A_2$  values. One of the reasons for these differences is the underestimation of the photopeak efficiency values at 1173 and 1332 keV. This underestimation primarily results from the definition of the photon source in the calculation. We defined only the cells of the armor tiles as photon sources in the MCNP calculations; however, every component was activated in the deuterium experiments and was not considered. In particular, the half-life of  $^{60}\text{Co}$  was approximately

5.271 years, which was longer than those of  $^{58}\text{Co}$  and  $^{54}\text{Mn}$  (70.86 and 312.03 days, respectively).  $^{60}\text{Co}$  possibly lingered around the devices, and discrepancies occurred between  $A_1$  and  $A_2$ . Moreover, the replacement of armor tiles was not considered in this study, which is one of the reasons for these discrepancies.

## 5. Conclusion

Activation analysis was conducted using a P-HPGe detector inside the LHD vacuum vessel, and the measured results were compared with those of the removed armor tiles. The following results were obtained.

- (1) The radionuclides  $^{58}\text{Co}$ ,  $^{54}\text{Mn}$ , and  $^{60}\text{Co}$  were measured, and the results were the same as the previous findings obtained by removing the armor tiles
- (2) The activities of  $^{58}\text{Co}$  and  $^{54}\text{Mn}$  measured inside the LHD vacuum vessel were consistent with the results for the removed armor tiles, whereas the activity of  $^{60}\text{Co}$  was higher than that obtained from the removed armor tiles. This discrepancy was due to the type of reaction, half-life, and frequency of replacement of the armor tiles

Based on these observations, activation by fast neutrons can be measured using this method; however, the reason for the activation by fast neutrons must be clarified. Moreover, the discrepancy in the activities indicates that gamma-ray transport from the outer region of the vacuum vessel is important for the overall estimation of the radiation dose.

## Data Availability

The measured data and input file for the calculation used to support the findings of this study are available from the corresponding author upon request.

## Conflicts of Interest

The authors declare that there is no conflict of interest regarding the publication of this article.

## Acknowledgments

This work was supported by the LHD experiment group and the LHD project budget (ULGG801, 10201041UPSX003-1, UPSX001-4, and ULEK702). This work was also performed with the support and under the auspices of the NIFS Collaboration Research Program (NIFS18KESA030 and NIFS19KLPA001).

## References

- [1] G. W. Bailey, O. V. Vilkhivskaya, and M. R. Gilbert, "Waste expectations of fusion steels under current waste repository criteria," *Nuclear Fusion*, vol. 61, no. 3, article 036010, 2021.
- [2] S. M. Gonzalez de Vicente, N. A. Smith, L. el-Guebaly et al., "Overview on the management of radioactive waste from fusion facilities: ITER demonstration machines and power plants," *Nuclear Fusion*, vol. 62, no. 8, article 085001, 2022.
- [3] P. Andrew, P. D. Brennan, J. P. Coad et al., "Tritium retention and clean-up in JET," *Fusion Engineering and Design*, vol. 47, no. 2-3, pp. 233–245, 1999.
- [4] Y. Katoh, D. Clark, Y. Ueda et al., "Progress in the U.S./Japan PHENIX project for the technological assessment of plasma facing components for DEMO reactors," *Fusion Science and Technology*, vol. 72, pp. 1–11, 2017.
- [5] Y. Nie, J. Ren, X. Ruan et al., "The benchmark experiment on slab beryllium with D-T neutrons for validation of evaluated nuclear data," *Fusion Engineering and Design*, vol. 105, pp. 8–14, 2016.
- [6] M. Osakabe, H. Takahashi, H. Yamada et al., "Recent results from deuterium experiments on the large helical device and their contribution to fusion reactor development," *Nuclear Fusion*, vol. 62, no. 4, article 042019, 2022.
- [7] H. Nakanishi, M. Yokota, M. Aoyagi et al., "Integrated radiation monitoring and interlock system for the LHD deuterium experiments," *Fusion Engineering and Design*, vol. 129, pp. 259–262, 2018.
- [8] M. Kobayashi, T. Tanaka, T. Nishitani et al., "Neutron flux distributions in the Large Helical Device torus hall evaluated by an imaging plate technique in the first campaign of the deuterium plasma experiment," *Nuclear Fusion*, vol. 59, no. 12, article 126003, 2019.
- [9] M. I. Kobayashi, N. Suzuki, T. Saze et al., "The evaluation of a simple measurement method using NaI(Tl) scintillation survey-meter for radiation safety management of radioactivated armor tiles of LHD vacuum vessel," *Radiation Safety Management*, vol. 20, pp. 20–28, 2021.
- [10] T. Goorley, M. James, T. Booth et al., "Initial MCNP6 release overview," *Nuclear Technology*, vol. 180, no. 3, pp. 298–315, 2012.
- [11] T. Nishitani, K. Ogawa, and M. Isobe, "Monte Carlo simulation of the neutron measurement for the Large Helical Device deuterium experiments," *Fusion Engineering and Design*, vol. 123, pp. 1020–1024, 2017.
- [12] W. White, *Photoatomic data library MCPLIB04: a new photoatomic library based on data from ENDF/B-VI release 8*, Los Alamos National Laboratory, 2003, <https://nucleardata.lanl.gov/ace/mcplib04/>.
- [13] Y. Nobuta, S. Masuzaki, M. Tokitani et al., "Effects of modified surfaces produced at plasma-facing surface on hydrogen release behavior in the LHD," *Nuclear Materials and Energy*, vol. 12, pp. 483–487, 2017.
- [14] M. Tokitani, N. Yoshida, M. Miyamoto et al., "Characterization of surface modifications of plasma-facing components in LHD," *Fusion Science and Technology*, vol. 58, no. 1, pp. 305–320, 2010.
- [15] K. Shibata, O. Iwamoto, T. Nakagawa et al., "JENDL-4.0: a new library for nuclear science and engineering," *Journal of Nuclear Science and Technology*, vol. 48, no. 1, pp. 1–30, 2011.
- [16] Y. Ikeda, Y. Seki, H. Maekawa, Y. Oyama, and T. Nakamura, "Measurements of induced activity in type 316 stainless steel by irradiation in D-T neutron fields," *Fusion Technology*, vol. 8, no. 1P2B, pp. 1466–1471, 1985.
- [17] T. Tanaka, S. Yoshihashi, M. Kobayashi et al., "Measurement of neutron spectrum using activation method in deuterium plasma experiment at LHD," *Fusion Engineering and Design*, vol. 146, pp. 496–499, 2019.
- [18] Y. Ikeda, A. Kumar, C. Konno et al., "Measurements and analyses of decay radioactivity induced in simulated deuterium-tritium neutron environments for fusion reactor structural materials," *Fusion Technology*, vol. 28, no. 1, pp. 74–98, 1995.
- [19] M. R. Tomaz Zagar, "Measurement of neutron activation in concrete samples," in *Int. Conf. Nucl. Energy Cent. Eur. -2000*, pp. 1–8, Bled, Slovenia, 2000.
- [20] H. Matsumura, A. Toyoda, K. Masumoto et al., "In-situ determination of residual specific activity in activated concrete walls of a PET-cyclotron room," *Journal of Physics: Conference Series*, vol. 1046, article 012016, 2018.